2024-04

Impacts and prospective hazard analysis of rainfall-triggered lahars on St. Vincent 20212022

Phillips, J

10.1144/sp539-2022-313
Geological Society, London, Special Publications
Geological Society of London

Accepted Manuscript

Geological Society, London, Special Publications

Impacts and prospective hazard analysis of rainfall-triggered lahars on St. Vincent 2021–2022

Jeremy Phillips, Jenni Barclay, Paul Cole, Monique Johnson, Victoria Miller & Richard Robertson

DOI: https://doi.org/10.1144/SP539-2022-313

To access the most recent version of this article, please click the DOI URL in the line above. When citing this article please include the above DOI.

Received 2 November 2022
Revised 17 July 2023
Accepted 1 August 2023

Impacts and prospective hazard analysis of rainfall-triggered lahars on St. Vincent 2021-2022

Jeremy Phillips[1,*], Jenni Barclay[2], Paul Cole[3], Monique Johnson[4], Victoria Miller[5], Richard Robertson[4]

[1] School of Earth Sciences, University of Bristol, Wills Memorial Building, Queens Road, Bristol BS8 1RJ, UK

[2] School of Environmental Sciences, University of East Anglia, Norwich Research Park, Norwich NR4 7TJ, UK

[3] School of Geography, Earth and Environmental Sciences, University of Plymouth, Plymouth PL4 8AA, UK

[4] The University of the West Indies, Seismic Research Centre, St Augustine, Trinidad and Tobago, West Indies

[5] GNS Science, P.O. Box 30368, Lower Hutt, 5040, Aotearoa New Zealand

* Corresponding Author J.C.Phillips@bristol.ac.uk

Abstract

Lahars are energetic flows of loosely consolidated volcanic debris and water, which have occurred frequently after rainfall events on St Vincent in the Eastern Caribbean since the April 2021 explosive phase of the 2020-21 eruption of La Soufriere volcano. Using scientific observations and information from social media, we have constructed a detailed timeline of the 25 lahar events that occurred during 2021, and summarised lahar impacts and losses. 20 mm daily rainfall on a river catchment is (and remains) sufficient to result in a lahar. We used this threshold, with field estimates of lahar volumes, to conduct both an island-wide assessment of potentially impacted locations using the LAHARZ model, and a detailed reconstruction of one lahar event, using the dynamic model LaharFlow. A simplified catchment hydrology approach with runoff ratios typical for the Caribbean showed good agreement with observations of flow properties near the coast.

Lahars will continue to be an important hazard in St Vincent into the future, and our modelling approach can assess future lahar impacts and provide early warnings. Social media provided key information about lahars and impacts, and allowed communities to alert each other. Future hazard mitigation should strengthen links between communities and with national risk management.

'Lahar' is a term of Indonesian origin and describes flows that involve a mixture of loosely consolidated volcanic debris and water occurring on and around volcanoes (Vallance, 2005). All of the volcanoes of the Eastern Caribbean are susceptible to lahars following explosive eruptions as a consequence of intense rainfall during rainy seasons in the tropical climatic zone where they are located. These are generated by the interaction of intense, frequent rainfall with the resultant loosely consolidated deposits either from tephra or pyroclastic density current deposits. La Soufrière volcano (St. Vincent) generated a series of explosions between the 9th and 22nd of April 2021, following approximately three months of effusive activity, confined to a summit crater without a substantive lake. There were at least 24 discrete explosions and one prolonged period of fluctuating but continuous explosive activity (Joseph et al, 2022a; Sparks et al, this volume). This generated island wide tephra, and from approximately 18:30 UTC on the 10th of April these explosive events also generated pyroclastic density currents (PDCs) that flowed down multiple drainages leading from the summit crater (Cole et al, this volume). Tephra was unevenly dispersed across the island (in both thickness and median diameter) with distal coastal locations to the south and east only receiving a few mm of fine-grained ash during a subset of the early explosions. Some villages in proximal coastal locations in the northeast received tephra for most of the eruptive sequence, resulting in deposits greater than 100 mm in thickness (Cole et al, this volume). PDCs reached to 4.2 km to the west and to 2.8 km to the south with tephra thicknesses at 3 to 4 km distance > 100 mm, increasing rapidly towards the crater (Cole et al, this volume). These deposits and flows were also associated with substantive vegetation damage later evidenced in the make-up of the lahar deposits.

Both syn-eruptive and post-eruptive lahars have been observed in the historical and near historical past across the Eastern Caribbean. For example, recent analysis of historical lahar occurrence on Mount Pelee and La Soufriere (Guadeloupe) recorded some 165 syn-, post- and non-eruptive lahars between 1530 and 2009 although substantial peaks in lahar occurrence are associated with Pelée's eruptive activity in 1902 and 1939 (Leone et al, 2019). Longitudinal analysis of catchment response to the perturbations associated with the 1995-2010 eruption of Soufriere Hills Volcano, Montserrat (Barclay et al, 2007, Christie et al, in prep) demonstrate the long wavelength disturbance of these systems, responding variously to intense precipitation and seasonal variation in ground saturation, vegetation loss and the input of a heterogenous variety of sediment. The difference between lahars and flash-flooding on these tropical islands in terms of outcome via damage impacts is indistinct so here we consider a 'lahar' to be any water-saturated sediment-charged flow associated with the transport and incorporation of loose volcanic material (whether recently erupted, 'syn' and 'post' or via excavation of unconsolidated volcanic deposits 'non-eruptive'). The lahars considered here can be debris flows, hyperconcentrated streamflow or streamflow and often transition between these flows states during any one event.

On St. Vincent both the 1902 and 1979 explosive events at La Soufriere were initiated in the presence of a substantive crater lake, and this has been implicitly attributed to the generation of syn-eruptive lahars. In 1902 contemporary accounts of the opening phases of the paroxysmal 7th of May eruption involve variously accounts of boiling flows, and some field evidence indicates that lahars are preserved locally near the base of the 1902 sequence (Cole et al, 2019). Following these eruptions initial rainfall percolated into the thick PDC deposits but only generated localised explosions rather than debris-charged water flow (Hovey, 1909). By March 1903 the '*immediate gorge of the Wallibou had been mostly cleared of its filling of ash*' (Hovey, 1909, p.421) by lahars, and dilute sediment-water flows were occurring, initiated by dry landslides from the destabilised

slopes of the valley. A further visit in 1908, remarked on the still-disturbed geomorphology of these valleys and included the direct observations of debris-charged flows occurring after rainfall which '*brought the river down on the surface of its bed to the sea in pulsations overloaded with debris and easily rolling along boulders in 30 or more centimeters in diameter*' (Hovey, 1909, p.421). These flows were observed in both the Rabaka (sic) and the Wallibou. At this point there was still substantive modification to the shoreline with ongoing processes of coastal erosion that Hovey (1909) inferred would eventually return to that of the pre-eruptive morphology. In 1979 'mudflows' were reported during the initial vulcanian explosive phase (13th to 26th April) alongside the generation of base surges and minor PDCs. Initial explosions breached a pre-existing dome in the crater lake with the consequent ingress of water into the vent influencing the style of later explosions, until the crater lake disappeared (Fiske and Sigurdsson, 1982). However, there is less record of laharic activity following these eruptions, although the 5 short-lived explosions only generated limited source material; PDC deposits were confined to valleys within 2 km of the crater and the cumulative deposit was only 30-40 mm at distances of 3 to 4 km from the vent (Sigurdsson, 1982).

Lahars were observed during the short explosive phase of the 2020-21 eruption of La Soufriere volcano, and have continued to occur until the time of writing. The first lahar was reported on 11th April 2021, and subsequently lahars were detected by the seismic network and observed in all valleys around La Soufriere. (Joseph et al, 2022b) Their impacts were particularly felt by resident communities on the Windward (east) side of the island, where the only road to the north around the coast crosses several rivers including the Rabacca and Overland rivers, and rivers in the settlements of Sandy Bay, Owia and Fancy (Fig. 1). The expectation from previous eruptions of La Soufriere and from climate projections showing more intense rainfall for the Caribbean (both during and outwit large weather systems associated with the May to November hurricane season; Taylor et al, 2012) is that lahars will continue to be a significant hazard on St Vincent into the future.

In this work we will synthesize a catalogue of lahar events during 2021, and review their impacts. Their detection on the seismic network cannot identify which valley they are flowing down, so we also use journalistic and social media records as well as discussions in local community WhatsApp chat groups. Recording small and relatively frequent lahar events is a challenge as the steep and sometimes denuded topography in the volcanic region of the island means that communities in St Vincent are used to the impacts of seasonal flash flooding which is not dissimilar to lahars. So, recording of events is typically unsystematic and variable in detail. There were also some challenges due to the short duration of the eruptive phase and in accessing the field areas during this time. Consequently, the focus of this paper is not on providing a detailed field stratigraphy of individual lahar events, rather we use parts of these field data as the basis for estimating the volume of future events for input to hazard models that predict their impacts.

The aim of this paper is to use our analysis of the drivers and outcomes from lahars to date, combined with models of lahar inundation within the context of past behaviour in this or analogue settings to suggest a pathway for anticipating and potentially mitigating the impacts of future lahars in St Vincent. This builds on the first order-assessment presented by Miller et al (2022). To do this we will construct a database of lahar events and correlate this with triggering rainfall, use observations of lahar events and their impacts to estimate the lahar volumes and volume fluxes to provide initial conditions for lahar hazard modelling. We present some preliminary results from this work with a

discussion of how this can be used to contribute to early warnings and preparedness planning for future lahar impacts on St Vincent.

Observations and Impacts of Lahars

Timeline of Lahar Occurrence and Rainfall during 2021

A database of lahar events from the start of the eruption until the end of 2021 was compiled to characterise their location and scale, using observations made by scientists working in the field, detections of lahars on the seismic network, and reports in newspapers and social media. The database indicated that lahars were observed or instrumentally detected on 25 days during this period. Lahar observations were made on 14 days by scientists from Belmont Observatory (Fig. 1) working in the field, and reported in Scientific Advisories and local newspapers (Scientific Advisories are official reports summarising observations and their interpretation by the monitoring scientists, and those for the 2020-2021 eruption are collected by Joseph et al, 2022b). Since May 2021, lahars have also been detected on 16 days on the seismic network, and reported in Scientific Advisories. The first mention of possible lahar activity is in Scientific Advisory 202011_SVG_44 on 11th April, noting 'steaming in the upper parts of the Rabacca valley' as under investigation. Subsequent reporting of lahars in the Scientific Advisories mostly notes that lahars were detected on the seismic network, sometimes indicating the location of the strongest signals, but not identifying specific valleys down which lahars travelled. Lahars were also reported in the online newspapers iWitness News , Searchlight and the Barbados Advocate. These reports mostly quoted National Emergency Management Organisation (NEMO) officials or the University of the West Indies Seismic Research Centre (SRC) scientists describing lahar events, sometimes from the daily 8 am National Broadcasting Corporation radio programme 'Eyeing the Volcano'. Photographs of lahars were occasionally included, typically uncredited and undated but sometimes including the location.

Community observations of lahars, shared on social media, were also an important source of information for constructing the timeline of lahar events. Between September 2021 and April 2022 a community engagement project, 'Changing Landscapes', was set up as part of the United Kingdom Research and Innovation Global Challenges Research Fund 'Risk at the Margins' research project. The project involved communities from the northeast of St Vincent, the areas most affected by the eruption and lahars. One of the activities of the project included workshop discussions on the utility of documenting lahar events particularly at river crossings and the value of community knowledge for improving scientific understanding of St Vincent lahars. After the workshop, the Changing Landscapes project participants formed a WhatsApp group where they shared social media links to photos and video recordings of significant lahar events from their community network. Between April 12th and August 30th 2021, video recordings of 18 lahars were shared on social media platforms by residents of the north windward communities across 9 different river crossing locations. From January to September 2022, 5 additional lahar observations were retrieved from the Changing Landscapes WhatsApp Group including videos and written reports of lahars at the Overland River crossing (Fig. 1). These observations were correlated with rain gauge observations and instrumental data to populate the database and confirm locations of lahar occurrences. They were also useful for constraining timings and characteristics of lahar flow to support modelling of future impacts.

In our analysis, we compare timings of lahar occurrence with rainfall records, using daily rainfall totals from 25 raingauges located across St Vincent and managed by the Central Water and

Sewerage Authority (CWSA) of St Vincent and the Grenadines (Fig. 1). We explored the correlation between lahar occurrence and daily rainfall total, using both the daily rainfall total from the raingauge nearest to the location of the lahar event (if known) and the maximum daily rainfall total recorded on any of the raingauges. Daily total rainfall is the highest resolution available, so our analysis is consistent with some recent approaches for characterising the initiation of lahars by rainfall, which use constant rainfall rates for the duration of rainfall events over daily or multi-day timescales (Mead et al, 2016; Baumann et al, 2018). We recognise the shortcomings of being limited to daily rainfall data since lahar initiation depends on both rainfall intensity and duration, as has been shown in previous studies (Rodolfo et al, 1996; Lavigne and Thouret, 2003; Van Western and Daag, 2005). Jones et al (2015) show that peak rainfall in one hour is a better predictor of lahar occurrence than total daily rainfall for temperate moderately vegetated land cover at Tungurahua volcano Ecuador. In line with our analysis, they also show that antecedent rainfall (1, 3 and 5 days before recorded lahar events) is not an effective predictor of lahar occurrence when used in isolation, but improves forecasts of lahar events when combined with peak one-hourly rainfall. The aim of our analysis is not to identify a formal threshold for issuing early warnings of lahar events, which would need higher resolution rainfall measurements (c.f. Jones et al, 2015), rather here we use the comparison between lahar occurrence and daily rainfall totals to infer the initial conditions for lahar initiation and modelling, aimed at supporting longer-term preparedness and mitigation planning.

A timeline of lahar occurrence and daily rainfall is presented as Fig. 2, which shows schematically the occurrence and observed extent of lahar events, and peak national and local daily rainfall, from which we can draw out broad trends in the correlation between rainfall and lahar occurrence in 2021. During 2021, lahars occurred in all valleys around the volcano. On the 14 days in which lahars were directly observed, on eight days lahars were reported around all or most valleys on the volcano, on two days lahars were reported only on the west side, on one day lahars were reported only on the east side, and for three days there is insufficient information to identify lahar locations. No information on lahar location or direction is reported in the Scientific Advisories. Over the period April to November 2021 there were two significant rainfall periods, on 27th April to 5th May, and 20th to 25th August, during which it is likely that lahar occurrence depended on antecedent rainfall on preceding days as well as on the days when events were observed or instrumentally detected. Lahar observations and rainfall measurements are presented as Table 1.

The first lahar was reported on 11th April (two days after the start of the eruption). There was relatively low rainfall on this day (national maximum of 9.4 mm in the central south of the island recorded at Montreal) and approximately 5 mm on both the west (Dallaway) and east (Jennings) sides of the island (all raingauge locations are shown on Fig. 1). There was also little antecedent rainfall (maximum daily rainfall of 6.3 mm anywhere on St Vincent in the preceding two days), so this event is likely mobilisation of fresh and unconsolidated pyroclastic deposits by relatively low rainfall.

For lahar events from late April 2021 onwards, we can identify consistent trends in the correlation of their occurrence and daily rainfall. On days on which lahars occur in one, or a few, valleys on the same side of the volcano, a minimum of about 20 mm of daily rainfall was measured in raingauges local to the lahar location. On days when lahars are observed in all or most valleys around the volcano (associated with the significant rainfall periods in April and August), there is both daily rainfall in excess of 80 mm anywhere on St Vincent, and rainfall near the volcano (either west or east

sides) of at least 55 mm. The exception to this is for three later days (5th and 6th May and 21st August) within the two significant rainfall periods mentioned earlier, when lahar occurrence was correlated with lower daily rainfall (minimum 5.8 mm daily anywhere on St Vincent), although the previous one or two days had high daily rainfall and indicated the importance of antecedent rainfall on lahar initiation. On days on which lahars were detected on the seismic network (with no information about the valley in which the occurred), there was a minimum daily rainfall of about 20 mm or more measured close to valleys known for lahar activity since the start of the eruption.

From this limited analysis we conclude that lahar initiation is associated with at least 20 mm daily rainfall measured close to the lahar route, and this threshold has not changed during the first seven months after the eruption. Larger rainfall events can trigger lahars in multiple valleys around the volcano, with the same threshold rainfall observed for April and August 2021. Typically, lahar initiation requires increasing rainfall totals with time after the eruption, as pyroclastic deposits harden and form less permeable crusts due to chemical weathering (Baumann et al, 2018; Yamakoshi, 2005); this does not appear to be the case over the first seven months since the eruption in April 2021, and suggests that the lahar hazard may be significant on St Vincent for some time into the future.

Lahar Deposits

Syneruptive lahars

Syneruptive lahars occurred in at least the Wallibou and Dry Wallibou valleys on 11th April. These valleys are to the west of the volcano (Fig. 1) and are so named because the Dry Wallibou only has an active channel during the rainy season (typically June to November), whereas the Wallibou has an active channel throughout the year. The deposits from these events were examined on 26th April, 4 days after the explosions had ended, and were locally still warm to touch. These deposits were relatively fine-grained, at least on most of their surfaces (Figs. 3a and b). The deposits had apparently extended across the whole valley rather than being channelized. Small wooded areas at the margins of the Wallibou valley were inundated by the lahars to depths of between approximately 1 and 2 m (Fig. 3a). Flow fronts were either similarly fine-grained with small lobes 10s of cm high (Fig. 3a), or composed of collections of tree trunks and branches (Fig. 3b). Locally, particularly at flow fronts near the coast of the Wallibou areas were concentrated in scoria blocks ~ 20 cm in size. The surface of the syneruptive lahar deposit both in the and Dry Wallibou valleys contained extensive 'dessication cracks' that appear to have been deformed by continued creep of the deposit following emplacement (Fig. 3c). All evidence indicates that these syneruptive lahars were wholly depositional rather than erosive.

Sections through the syneruptive lahar deposits showed a generally massive, non-stratified nature, although of two or three separate units could be identified (Fig. 3d). These massive deposits were up to ~10 m thick in total in the lower parts of the Wallbou valley. Thicknesses in the Dry Wallibou were thinner, ~ 1m thick. Tephra fallout from the explosive activity was observed below these lahar deposits in ~~both~~ the mouths of both the Dry Wallibou and Wallibou valleys (Fig. 3c) confirming the timing of these deposits occurring at least after the initial activity on 9th and 10th April.

Post Explosion lahar deposits

Significant lahar events were observed in the Wallibou valley on 29th April and 3rd May 2021. The 29th April lahars generated significant erosion through the syneruptive lahar deposits in the lower 500 m of the Wallibou valley: originally flat fans at the shoreline of both the Wallibou and Dry Wallibou valleys formed by the syneruptive lahars (on 11th April) were deeply dissected. Those on 3rd May were also notably erosive, widening the canyons and eroding the older (pre 1902) pre-exiting pyroclastic deposits in the walls of the Wallibou valley.

Deposits formed on the 29th April, 3rd May and later events differed significantly from those of the syneruptive lahars. These deposits filled channels and valleys cut into the extensive, valley-wide terraces formed by the syneruptive lahars on 11 April (Fig. 3e). The deposits typically showed centimetre to millimetre scale discontinuous lensoid bedding, characterised by coarser lenses up to ~20cm thick and finer-grained, millimetre scale, cross laminated lenses. Very fine ash was generally lacking from these deposits (Figs. 3e and 3f).

Estimates of Lahar Volume from Field Observations

A lahar event on 3rd May 2021 was observed in detail from a vantage point above the lower Wallibou valley at location [13.313, -61.231] close to Richmond Vale Academy (location shown as 'Richmond' on Fig. 1). The flow lasted approximately one hour from 11.30 to 12.30 local time, and video recordings of the flow were made intermittently during this time. The flow consisted of a baseflow during which the channel base was sometimes exposed, allowing flow depth to be estimated, and intermittent pulses of higher flowrate (Fig. 4). Every few minutes, small pulses of increased flow rate were observed. These lasted about 30 s during which the flow depth increased by a factor of about 2. Less frequently, larger pulses that lasted a few minutes and increased the flow depth by a factor of 2 to 4 were observed (Fig. 4b). The flow was predominantly fine-grained sediment with intermittently larger boulders of 10s cm to 1 m scale visible in the flow, primarily during higher flowrate pulses. Bank undercutting and erosion of previous lahar deposits at the channel edges was observed.

We estimate approximately the mean discharge over the event using field estimates of vegetation dimensions to constrain the channel width and flow depth from video imagery of the lahars. We estimate a channel width of between 15 and 30 m (Fig. 4a), flow depths and velocities of between approximately 0.3 m and 0.5 m and 2 m s^{-1} and 3 m s^{-1} for the lower discharge continuous baseflow, and flow depths and velocities of approximately 1 m and 4 m s^{-1} for intermittent pulses of higher discharge. These flow conditions correspond to discharge estimates from 10 to 45 m^3 s^{-1} for the baseflow, corresponding to a lahar volume estimate of between 4×10^4 and 2×10^5 m^3 due to the steady component of the flow. Field observations suggested the flow conditions for the high discharge pulses were maintained for about 10% of the duration of the lahar event, giving an estimate of total lahar volume of between 5×10^4 and 2×10^5 m^3. The pulsatory nature of the flows makes estimation of the lahar volume from flow observations challenging, so these volumes should be treated as order of magnitude estimates.

Lahar impacts

The explosive phase of the eruption drastically altered the hydrological system of the watersheds, as vegetation was damaged or destroyed by ballistic projectiles, PDCs and heavy tephra falls which resulted in destruction of the forest (particularly on the upper parts of the volcano) and removal of

the protective ground cover. This caused increased runoff on the steep terrain, triggered by high-volume and long-duration rainfall events that occurred after the eruption. Rapid erosion and transport of loose volcanic materials downslope by lahars was both spatially and temporally controlled as most of the physical damage was concentrated in areas located on the flanks of the volcano and was most significant soon after the eruption ended when tephra thickness was highest.

The radial nature of the drainage and damage to vegetation on the upper flanks of the volcano resulted in lahars occurring on all flanks of the volcano. This meant that the primary coastal road was most vulnerable to lahar inundation along the multiple river ford and bridges that connect communities. As such the physical impacts of lahars was most visible at river crossings where there was damage caused to houses, roads, bridges, fords and electrical infrastructure (~US$12M for total damage; Government of St. Vincent and the Grenadines, 2021a). Less visible was damage caused to water and electricity supply and distribution infrastructure which rely on surface water intakes from rivers. Lahars caused damage to spring intakes, reservoirs, and pipes especially infrastructure that was exposed above ground or located near to flow paths. They destroyed the catchment systems for water at Sandy Bay, Owia and Fancy (all located on the volcano; see Fig. 1), including river intake, pipelines and treatment tanks. Damage to the water supply infrastructure at Fancy, Owia and Sandy Bay including major damage to catchment intake structures and pipelines amounted to an estimated XCD$241K (Government of St. Vincent and the Grenadines, 2021b). An additional XCD$63K in damages was reported to water catchment systems at Perseverance and Jennings (see Fig. 1) (Government of St. Vincent and the Grenadines, 2021b). Disruption of supply to residents in various catchment systems resulted in losses ranging from EC$115K to EC$210K (Government of St. Vincent and the Grenadines, 2021b). In addition to damage to electricity poles, lahars also affected power generation due to the clogging of intake structures leading to the Richmond, Cumberland and South Rivers Hydro-electric power stations (see Fig. 1) by debris brought down in the rivers. This impact was most severe at the Richmond Power Station which was out of commission for 16 weeks following the eruption due to physical damage from lahars.

In examining the systemic impacts of lahars consideration must also be given to the loss of functionality as well as cost and duration of repairs which are in turn related to their direct physical impacts. Lahars damaged electrical poles and water intakes and so disrupted both water supply and electricity supply to communities (Government of St. Vincent and the Grenadines, 2021c). Loss of function occurred as catchment systems were shut down or compromised due to increased turbidity. The damage from such impacts was most significant north of the Rabacca River (see Fig. 1) where lack of road access due to lahar damage hampered repairs to poles and lines that were damaged and down. Lahar impacts also required clean up support to allow access for repairs and cleaning. Of all the critical infrastructure sectors, transportation was the most severely impacted with an estimated cost of damage to bridges and river fords in the red and orange volcanic hazard zones (Fig. 5) amounting to approximately XCD$32.5 million (Government of St. Vincent and the Grenadines, 2021b).

Lahar damage to the Windward Highway (Fig. 5) severely limited the speed at which repairs could have been undertaken to water catchments and electricity supply. As such the impact of lahars extended beyond the direct physical damage to infrastructure and lasted longer than the specific period over which the events occurred. Disruption of the transportation network exacerbated disruption of the electrical and water systems by increasing the time for recovery and restoration of

these systems as the repair crews and equipment could not get to critical sites (e.g. watch catchments, storage tanks, fallen electricity poles) to conduct repairs.

Using Lahar and Rainfall Observations to Inform Hazard Modelling

In this section, we test the capability of two different modelling approaches to assess future lahar hazards and impacts on St Vincent. The first applies the widely-used lahar inundation model Laharz (Schilling, 2014) with volume estimates derived from observations of the 3rd May lahar in the Wallibou valley. The second uses a dynamic model for lahars with rainfall volume estimates for the Overland River catchment (see Fig. 1). Lahars in this location are typically dilute, so we do not attempt to model initiation by shallow landsliding as in previous studies (e.g. Mead et al, 2016; Baumann et al, 2018), but instead take a simplified approach using a runoff coefficient (the ratio of rainfall runoff to total rainfall), which is widely used for flash-flooding on steep catchments (e.g. Tarolli et al, 2012). We use runoff coefficients from 0.2 (as suggested for national-scale flood hazard assessment in St Vincent; CHARIM, 2014) to 0.65 (as inferred for steep tropical catchments in Costa Rica; Garcia-Martino et al, 1996), noting that this value is poorly-constrained and will increase with pre-event rainfall or wetness (Longobardi et al, 2003; Ogden, 2016).

Scenario modelling of lahar inundation as a guide for hazard assessment

A first-order assessment of lahar hazard footprints was undertaken using Laharz (Iverson et al., 1998; Schilling, 2014), a widely-used tool for understanding potential lahar inundation zones, to obtain an overall picture for future lahar impacts within the high hazard zone in the northern part of St. Vincent (Fig. 6). The Laharz toolkit is a simplified tool for estimating inundation zones that is based on a statistical analysis of field-constrained lahar extents/volumes (Iverson et al., 1998) and flume experiments. It does not account for dynamic lahar processes, but rather assumes all of the parameters are constant during a given lahar event. Despite being a simplified model, Laharz has been widely implemented due to its ability to rapidly generate first-order inundation models with multiple user-defined lahar volumes simultaneously (e.g. Darnell et al., 2012; Castruccio and Clavero, 2015). Here we employ the Laharz plugin for the ArcGIS software (Schilling, 2014).

The required inputs for Laharz are a digital elevation model (DEM) and input lahar volume(s) to produce a drainage network and initiation points; the model then uses a pair of statistically derived empirical equations that relate the volume with the cross-sectional and planimetric areas to estimate potential inundation areas. The ability of the DEM to adequately represent topography is a function of its resolution and age (i.e. how much the land surface may have changed since the DEM was developed). Initial lahar volume can be estimated from measured events at a particular volcano and/or using a range of estimated volumes based upon historic lahar events in similar settings. Individual initiation points can be identified and used in the modelling when detailed knowledge of the drainage system is available, with this providing the additional advantage of reducing the computational requirements of the simulation. A proximal hazard zone is calculated in Laharz based on the height/runout length (H/L) slope value, whereby the intersection of this boundary with river channels provides initiation points. This (H/L) value is often linked to breaks in slope, which should define the area that is most likely to be affected by primary volcanic activity (Schilling, 2014). Griswold and Iverson (2008) described H/L as the boundary where lahar behaviour changes from predominantly erosive to mainly depositional.

Here the 15-m DEM generated in 2005 by SRC (Robertson, 2005) was used for scenario estimates of future lahar hazard to ensure a consistent resolution for the entire modelled area. The DEM was padded with 0-m pixel values beyond the shoreline of St. Vincent to prevent the premature termination of the Laharz simulation, which can occur if there is an inadequate runout distance for larger lahar volumes that propagate along the DEM surface. Laharz creates surface hydrology rasters to define the downstream movement of the hydrologic flows over the DEM surface using a stream threshold value. A proximal hazard zone was delimited using H/L, as defined by the energy cone, which essentially represents the slope of the volcanic flanks. Several estimates were undertaken using a suite of input lahar volumes (5.0×10^3, 5.0×10^4, 1.0×10^5, 5.0×10^5 m^3) to create a range of low to high estimates. Full details are provided in Miller et al (2022), and we note here that this progression of increasing lahar volumes is not geometric, as would be ideal for an empirical model calibrated on an exponential relationship as is the case for Laharz (see Iverson et al, 1998).

The modelled inundation using LAHARZ illustrates that the lahar hazard is confined to the north of St Vincent, the area of high volcanic hazard close to the volcano (Fig. 6). A comparison of the estimates of the calculated lahar flow for the Wallibou event on 3rd May 2021 (4×10^4 to 2×10^5 m^3) are consistent with the Laharz -derived runouts for 5.0×10^4 and 1.0×10^5 m^3 moderate volumes. We see that a volume of 5.0×10^4 m^3 is unable to reach the lower reaches of the Wallibou valley (Fig. 6b), whereas a volume of 1.0×10^5 m^3 can propagate to the coastline. In the absence of further volume estimates for lahars across the north of St Vincent, we can only consider these estimates as a guide for potential future scenarios in the other channels across the north of St. Vincent until lahar volume estimates are obtained for the other drainages. An examination of the Laharz estimates for the southernmost drainages on the eastern coastline indicate a similar pattern, whereby the events in the lower end of the simulated volume range ($<1.0 \times 10^5$ m^3) do not propagate to the lower portions of either the Waribishy or Rabacca channels, the Rabacca channel requiring much higher volumes to propagate to the coastline (Fig. 6a). However, the channels further north require much smaller initiation volumes to propagate to the lower reaches of their respective channels, which is where the population centres are typically located.

We note that the lahar inundation extent from a specific initiation point requires the mobilization of volcanic material via a minimum amount of localized rainfall; therefore, a given rainfall event is not expected to generate lahars from each of the identified initiation points, such that only a subset of the channel will be impacted at a given time. Again, it is important to note that the Laharz results should only be used as a guide due to the simplicity of the model, and the uncertainties in the underlying topographic model (DEM) and defined initiation points. If an updated DEM becomes available with more recent topography changes, then this analysis should be re-run. Manually selected initiation points for individual catchments would ideally be utilised as well. That said, the Laharz modelling approach is a useful tool for obtaining a first-order approximation of the likely hazard across this broad volcanic zone, which can be used as a guide for island-wide hazard mapping purposes and the creation of lahar awareness zones. However, more complex modelling tools should be considered if there is a requirement for detailed land-use planning or time-dependent outputs regarding lahar impacts.

Dynamic Modelling of lahars - the 8th December 2021 lahar at Overland

Recently available dynamic models for lahars and debris flows offer the capability to predict lahar flow depths and speeds and flow front arrival times, in addition to inundated area. These models, including LaharFlow (Woodhouse et al, 2016; Tierz et al, 2017), D-CLAW (Iverson and George, 2014), R-Avaflow (Mergili et al, 2017), Titan (Cordoba et al, 2015), Flo-2D (O'Brien et al, 1993) are formulated from conservation of mass and momentum of the flow, with a range of closures for frictional and material exchanges with the base, or rheologies. These models permit calculation of flow depths, densities and speeds, from which static pressure (the product of flow density, depth and gravitational acceleration) and dynamic pressure (the product of flow density and the square of the flow velocity) can be derived, to allow their impacts to be estimated (Jenkins et al, 2015; Gentile et al, 2022). In this study, we use the dynamic model LaharFlow (Woodhouse et al, 2016) which was developed and calibrated for lahars of a range of sizes, and explicitly parameterises processes of substrate erosion and deposition that are characteristic of lahars, and which are explicitly linked to evolution of topography and flow dynamics ~~in the model~~. Full details of the model have been presented elsewhere (Woodhouse et al 2016), although we present the formulation in summary form here for completeness. The model stability has been analysed (Langham et al, 2021), and it has been implemented as a webtool for use by operational hazard assessment agencies, available for download at www.laharflow.bristol.ac.uk .

LaharFlow model formulation

Laharflow solves equations of mass and momentum conservation under the 'shallow layer' assumption that underpins many surface flow models; the flow is 'shallow' (its length is much greater that its depth). This permits us to neglect slope-normal accelerations and average the flow motion over its depth, so that the lahar may be simulated efficiently over two spatial directions. The flow configuration is shown in Fig. 7; a layer of water containing solid particles flows down an arbitrary slope of elevation b. Its depth h, velocity $\boldsymbol{u} = (u, v)$, solids concentration C and the bed elevation b evolve as functions of space $\boldsymbol{x} = (x, y)$ and time t. We assume that the solids are well-mixed throughout the water column.

The model formulation consists of two mass conservation equations, for the particle-fluid mixture and for the particles separately, to explicitly compute changes in solid concentration by erosion and deposition. Conservation of the mixture mass is given by

$$\frac{\partial h}{\partial t} + \frac{\partial}{\partial x}(hu) + \frac{\partial}{\partial y}(hv) = E - D,$$

where E and D are rates of erosion and deposition respectively, which depend on the local flow state. Likewise, conservation of solid mass is given by

$$\frac{\partial}{\partial t}(hC) + \frac{\partial}{\partial x}(huC) + \frac{\partial}{\partial y}(hvC) = C_b(E - D),$$

where C_b denotes the volumetric concentration of solids in the bed. The two phases are assumed to move with the same depth-averaged velocity, $\boldsymbol{u}(x,y,t)$. The mixture density, ρ, is needed in order to form depth-averaged expressions for the evolution of momentum of the entire mixture. It is related to the concentration, C, and densities of the solid and fluid phases, ρ_s and ρ_f, respectively by $\rho =$

$\rho_f(1-C)+\rho_s C$. The momentum balances in each direction are written (e.g. Iverson and Ouyang, 2015; Peruzzetto et al 2021)

$$\frac{\partial}{\partial t}(\rho h\boldsymbol{u})+\nabla\cdot(\rho h\boldsymbol{u}\otimes\boldsymbol{u})+\frac{1}{\cos\theta}\nabla_s\left(\tfrac{1}{2}\rho g\cos^2(\theta)h^2\right)=-\rho hg\nabla_s b-\tau_b\frac{\boldsymbol{u}}{|\boldsymbol{u}|}+\nabla\cdot(\nu\rho h\nabla\boldsymbol{u}),$$

where θ is the angle between the slope normal and the direction of gravity, and $\nabla_s=\nabla-\boldsymbol{s}(\boldsymbol{s}\cdot\nabla)$, with $\boldsymbol{s}=\cos(\theta)\nabla b$, denotes the projection of the gradient operator onto the bed surface (after depth-averaging). On the right-hand side τ_b is the basal drag function and ν is an eddy diffusivity, whose inclusion ensures that the model possesses well-defined solutions (Langham et al 2021). The driving force is downslope gravitational acceleration (first term on the right-hand side), which is primarily balanced by the resistive stresses at the base of the flow (second term on the right-hand side). The spatial derivatives on the left-hand side comprise the expression for the rate of change of the momentum, which features the divergence of the momentum flux and the hydrostatic pressure gradient.

The evolution of the bed (which affects the topographic forcing on the flow) is controlled by the rates of erosion, E, and deposition, D at each point on the slope. It is modelled by

$$\frac{\partial b}{\partial t}=\frac{D-E}{\cos\theta}.$$

The factor of $1/\cos\theta$ on the right-hand is a geometric correction, accounting for the fact that bed elevation is measured along the vertical, while transfer of bed material takes place along the slope normal direction (Iverson and Ouyang, 2015).

The model is completed with closures for erosion, deposition and basal drag. Erosion is parameterised by analogy to bedload transport where the entrainment flux of eroded material is directly proportional to the excess basal stress (Meyer-Peter and Muller, 1948), and deposition flux is parameterised by analogy to hindered settling of particles from the flowing layer, using a settling law for geological particles in water (Soulsby, 1997) adjusted for hindered settling appropriate for high particle concentrations (Spearman and Manning, 2017; Richardson and Zaki, 1954). Basal drag terms are proposed which model the variation of flow resistance as the solid concentration varies. As lahars can span a wide range of solids concentration, from dilute flows with low concentration, through hyperconcentrated flows, to highly concentrated debris flows, the drag must capture pronounced changes in the resistance to motion. The basal drag is modelled as weighted contributions of fluid-like drag (at low concentration) and granular drag (at high concentration), with magnitude

$$\tau_b=\bar{\rho}\big(c_d|\overline{\boldsymbol{u}}|^2[1-f(C)]+\mu(I)ghf(C)\big).$$

This form is a generalization of Voellmy drag (Voellmy, 1955). Here $f(C)$ is a phenomenological '*switching*' function of the depth-averaged solids volume fraction $\bar{\psi}$, with

$$f(C)=\frac{1}{2}\big[1+\tanh\big(\lambda(C-C_0)\big)\big].$$

This form is a smooth function that transitions from small values $f(C)\approx 0$ for $C=0$ to $f(C)\to 1$ as $C\to C^*$ where $C^*\approx 0.6$ is the volume concentration at maximum packing. Therefore, in the dilute

limit $C \to 0$ the drag is dominated by the term $\tau_b \sim \bar{\rho} c_d |\overline{\boldsymbol{u}}|^2$, which is the Chezy form of drag used to model turbulent water flows (e.g. Chanson, 2004). The dimensionless parameter c_d is the Chezy drag parameter. In contrast, in the concentrated limit $C \to C^*$ the drag is dominated by the term $\tau_b \sim \bar{\rho} \mu(I) gh$, which is a Coulomb-like drag model for granular flows (see e.g. Forterre & Pouliquen, 2008), with $\mu(I) = \mu_1 + \frac{\mu_2 - \mu_1}{I_0/I+1}$, where $I = |\overline{\boldsymbol{u}}| d/h\sqrt{hg\cos\theta}$ is the dimensionless '*Inertial number*' (Forterre & Pouliquen, 2008) with d denoting the grain diameter. The parameter λ controls how rapidly the basal drag changes from fluid-like to granular resistance, while C_0 determines the volume fraction at which the transition occurs. The parameters μ_1, μ_2 and I_0 are material parameters, and $I_0 = 0.136$ is fixed. The various parameters in the description of basal drag, erosion and deposition have been calibrated against observations of lahars of various volumes (Woodhouse et al, 2016).

Application of LaharFlow to Lahar events in Overland River

We applied the model to simulate lahar events in the Overland catchment on the east side of St Vincent (Fig. 8). The main road to the north windward crosses the Overland River through a ford, so this is one of the critical locations for lahar impacts on the island. Notable lahar events reported by the local population and on social media happened here on 25th August 2021, 25th December 2021, 27th April 2022 and 1st July 2022. The first of these events resulted from multiple days of antecedent rainfall, with 105 mm rainfall recorded on 23rd August at the nearest CWSA raingauge at Jennings (Fig. 1; approximately 8 km from the Overland catchment). The other events resulted from intense rainfall on the day of the event, with 61 mm of rainfall on 25th December 2021 measured at Jennings, 41.2 mm rainfall on 27th April 2022, and 55 mm rainfall on 1st July 2022, both measured using a raingauge that was installed at Mahorne Ridge ([13.3196, -61.2126]; approximately 0.5 km from the Overland catchment) on 13th April 2022. These lahar events are of comparable volume and flow characteristics to that observed at Wallibou on 3rd May 2021 (Fig. 4), as shown in Fig. 9 for the 1st July 2022 lahar at Overland. The lahar is predominantly fine-grained sediment, with a flow depth and velocity ranging from 0.5 – 1 m and 1 to 3 m s^{-1} in the 20 m wide channel shown, and standing waves can clearly be seen on the right hand side (downstream direction) of the image. We estimate typical volume flowrates for these events in the range 10 – 60 m^3 s^{-1}.

The LaharFlow model uses an idealised initial condition of an instantaneous fixed volume release or a volume flux that varies over time (hydrograph), and can include multiple source locations and release times. However, unless there are detailed measurements of the lahar dynamics (including source locations and gauging of discharge, or quantitative observations from which to infer it), a standard approach as adopted here is to assume a simplified triangular (or 'three-point') hydrograph and explore sensitivity to that by model calibration (Woodhouse et al, 2016). The model requires a topographic map, and here we used a digital elevation map (DEM) generated as part of the charim project (CHARIM, 2014). This DEM had a resolution of 2 m for the channel in the lower part of the catchment (below the source location shown on Fig. 8) but was merged with coarser 30 m resolution mapping higher in the catchment. Simulations were run at a downscaled resolution of 5 m, which represents a compromise between longer run times at higher resolution, and sufficient grid cells across the typical channel width of 15 - 25 m.

To specify the source volume, we estimated the area of the Overland catchment and used a runoff ratio of 0.2 as suggested for national-scale flash flood assessment in St Vincent by the Charim project. Due to the DEM being merged from mapping at different resolutions, we could not use a GIS

algorithm to automate the measurement of catchment area, so we estimated this using 3-d projections of the catchment on Google Earth (Fig. 8) to identify the extent of the catchment based on downslope direction. This gave a catchment area of 2.82 km^2, which corresponds to a rainfall volume of 1.13 x 10^4 m^3 with our identified threshold of 20 mm daily rainfall and a runoff ratio of 0.2, increasing to 1.03 x 10^5 m^3 for the largest daily rainfall (of 61 mm) for the case study events and higher runoff ratio of 0.6 that has been inferred for more intense tropical storm rainfall in Dominica (Ogden, 2016). This is comparable to the volume range estimated for the 3rd May 2021 lahar in the Wallibou valley, but the lower end of the range is smaller for the Overland River. The Wallibou catchment has been estimated at 5.63 km^2 (Caribbean Conservation Association, 1991) which is larger than estimated for the Overland catchment, consistent with potentially larger volumes in the Wallibou.

Simulations were made with the LaharFlow model using triangular input hydrographs of a range of volumes and peak source volume fluxes. We used two criteria to assess whether the simulations were a good match to observed lahar events: the lahar travel time from the source to the Overland crossing (Fig. 8), and the flow conditions (flow depths, velocities and estimates of volume flowrate derived from these) reported at that location. The distance from the source to the Overland crossing is approximately 3 km, so flow travel times in excess of 120 mins correspond to mean flow velocities less than 0.4 m s^{-1}, which is inconsistent with both observations made at the Overland crossing (Fig. 9) and velocities typical of lahars in other locations in St Vincent (Fig. 4). Observations of lahar flow at the Overland crossing suggested that flow depths less than 0.5 m, flow velocities less than 1 m s^{-1} and volume fluxes outside the range 10 – 60 m^3 s^{-1} were unreasonable. Using these criteria, we found that source volumes of 1.13 x 10^4 m^3 were too small, and that a minimum source volume of 2.5 x 10^4 m^3 was needed, corresponding to a runoff coefficient of 0.44 and 20 mm of daily rainfall, or a runoff coefficient of 0.20 and 44 mm of daily rainfall. In addition, a peak source flux of 100 m^3 s^{-1} or more was needed to give reasonable travel times. Simulations at higher source volumes and fluxes up to 4.0 x 10^4 m^3 and 320 m^3 s^{-1} showed travel times in the range 80 – 110 mins. For the highest source volume, a rectangular hydrograph of constant source flux of 30 m^3 s^{-1} showed a travel time of 110 mins. In all cases, the source released water (a solids concentration of zero at the source), and the solids concentration changed during the flow as a consequence of erosion and deposition.

Outputs from the LaharFlow model are shown in Fig. 10 for one of the source conditions that was a good match to observations at the Overland crossing. Figs. 10a and 10b show the flow depth, which has maximum values of up to 5 m higher in the catchment. Fig. 10b shows an enlarged view of the flow depths at the Overland crossing, with values up to 1 m (orange cells) but mostly in the range 0.3 to 0.5 m (red cells). Fig. 10c shows the flow velocity (vector sum of along-channel and cross-channel depth-averaged velocities) with maximum values up to 3 m s^{-1} and most cell values in the range 1.5 to 3 m s^{-1}. Fig. 10d shows the topographic change at this time in the simulation, with red colours showing reduced cell heights (erosion), grey colours showing increased cell heights (deposition) and white showing height changes less than 10 cm. Erosion is observed primarily in the centre of channels, and on steeper topography, where there is faster flow, with erosion depths up to 2 m. There is relatively little erosion or deposition at the channel edges or on flatter topography close to the Overland crossing. Using the LaharFlow model, the increase of volume, or bulking, due to erosion, can be calculated from the computed erosion and a typical bed porosity. For simulations of lahars in the Overland catchment, bulking ranged up to a factor of approximately 1.3. This is on the

lower end of the range typical for lahar bulking (Vallance, 2000; Vallance and Iverson, 2015), consistent with the relatively small volume and short travel distance for this simulated lahar.

The use of paired criteria of matching observed flow conditions and volume flowrates at the Overland crossing constrained the model source parameter space to provide a reasonable starting point for simulating future lahar events on St Vincent. Note here that we have not varied the LaharFlow model parameter values for basal drag, erosion and deposition from their default values calibrated for a range of historical lahars (Woodhouse et al, 2016), in order to focus on inferring source conditions that produce flows consistent with observations. These parameter values could also be varied, but this would not increase the constraints on source conditions unless there were additional specific observations of erosion and deposition. We do not have observations of the lahar flow conditions at the Overland crossing for individual events on 25th December 2021, 27th April 2022 and 1st July 2022, so we cannot link source constraints to the rainfall on those days, but we can use these to infer a runoff coefficient range of 0.19 to 0.28.

Preparing for Future Lahar Impacts on St Vincent

The April 2021 eruption of St Vincent created conditions under which rainfall-triggered lahars have occurred repeatedly during heavy rainfall events since the eruption. The destruction of vegetation by the volcanic ash from tephra fall and pyroclastic density currents has resulted in increased rainfall runoff since the eruption, and remaining tephra deposits now provide a significant source of lahar materials. Our direct observations of lahar events, video postings of events on social media, and limited access to deposits on the western side, all suggest that the lahars are predominantly hyperconcentrated or concentrated streamflow, and only weakly erosive, as compared to typical lahars from larger eruptions (Pierson et al, 1990; Newhall and Punongbayan, 1996). Nonetheless, at the point of crossing the road the addition of sediment poses an additional extensive hazard to the populations in the northeast of St Vincent.

With the exception of the first few weeks after the eruption (where the lahars were more highly sediment concentrated and erosive), lahar inundation patterns and typical volumes have not changed significantly over the 25 events that occurred during the first 8 months after the eruption. A first-order assessment of lahar inundation, made using the Laharz model, suggests that these lahar volumes are sufficiently large to potentially cause impacts on populated coastal locations all around the volcano. Analysis of rainfall records shows that lahars can consistently be associated with as little as 20 mm daily rainfall proximal to the lahar source, although further work is needed to establish how robust this threshold rainfall is, as we have not analysed 'false positives' i.e. the number of times in the records that this rainfall is not correlated with a lahar event. Taken together, these results suggest that relatively small lahars can be triggered by relatively low daily rainfall, and their impacts on communities or infrastructure near river valleys are likely to constitute a significant hazard on St Vincent into the future.

The analysis and modelling conducted in this paper provides a starting point for mitigating impacts of future lahars through issuing of alerts, preparedness planning for areas likely to be inundated, and physical measures to protect infrastructure. In the immediate future, developing the existing CWSA raingauge network to provide higher temporal resolution rainfall measurements would allow 20 mm rainfall to be used as an effective threshold for lahar initiation to provide alerts to communities living in coastal regions or using river crossings. Independently of our analysis, the National Emergency

Management Organisation of St Vincent have reported at the UN Global Platform 2022 that 20 mm rainfall is sufficient to cause lahars (iWitness News, 2022) so this threshold already has importance for national risk management. Installation of additional high temporal-resolution raingauges close to critical infrastructure would improve capability to alert local communities. It has been demonstrated that in these small island settings significant orographic variation in rainfall can be anticipated for a range of weather systems (Barclay et al., 2006; Poulidis et al., 2016). By involving communities in the curation and collection of raingauge data in this region some progress has been made with this for communities in the northeast through the 'Changing Landscapes' project, but more coverage and long-term support for real-time raingauge networks is needed. In the meantime, working with communities to understand their experience of rainfall thresholds is critically important. Rainfall in St Vincent can be highly localised and rainfall in the lahar source regions does not always extend to the populated areas on the coast, but informal conversations with communities in the Northeast in Sandy Bay, Owia and Fancy, and analysis of social media posts indicates that people do know how heavy the rain needs to be for 'the river to come down' (i.e. a lahar event). The communication of warnings using social media platforms such as WhatsApp is an important short-term step for mitigation of lahar impacts and risk-to-life.

Longer term preparedness planning requires detailed characterisation of the dynamics of lahars to forecast inundation and impacts. The preliminary lahar modelling presented in this paper provides a framework for a more complete assessment of lahar threat in St Vincent in the future. The inundation modelling conducted using Laharz shows reasonable agreement with the observed lahar event in the Wallibou river on 3rd May 2021, and provides a rapid assessment of areas potentially inundated by future lahars, to enable prioritisation of higher-resolution dynamic modelling. Tests using the LaharFlow dynamic model on the Overland River catchment show that a simplified hydrological approach assigning a constant runoff ratio for rainfall onto a catchment can be used to set the initial conditions for simulations that show good agreement with observations of lahars at the coast. Using the 20 mm rainfall threshold, runoff ratios in the range 0.2 to 0.4 could be used as the basis for dynamic modelling of lahars in other catchments. In the absence of detailed hydrological models, which require comprehensive stream and rain gauging to implement, this simplified approach provides a starting point for characterising the dynamics and potential impacts of lahars. The dynamic modelling also provides a link between instrumental detection of lahars on the seismic network and warnings, as the models compute the travel time of the lahar through the catchment. Two of the Overland case study lahars (25th August 2021 and 1st July 2022) were detected on the seismic network at times before the flow reached the road crossing, and so there is potential with more detailed time recording of future events and modelling to quantify the warning time available from seismic detection of lahars.

Lahar impacts to the road network continue to be a significant source of disruption to communities in the northeast of St Vincent. Although these communities experience flash flooding from heavy rainfall that occurs during the rainy season, impacts from lahars are more significant, and the frequency and magnitude of lahar events since the end of the eruptive period on 22nd April 2021 has increased. Government response has been to construct bridges at the major river crossings, in essence shifting from the use of fords which was previously the dominant mechanism for roads crossing river valleys in the areas north of the Rabacca River. While the new bridges will alleviate the short-term issues, it is still important to assess potential lahar impacts to these bridge structures and other critical infrastructure include electricity poles, drinking water supply inlets and hydroelectric

power equipment situated in river channels. Dynamic modelling of sediment transport can anticipate impacts of future lahar events including bridge scour, loading on structures due to static and dynamic pressures exerted by the lahar flow, and blocking of pipework inlets.

Mitigating future lahar impacts will always require collaboration between scientific and risk management agencies and affected communities. Identifying which valleys and downstream communities lahars will impact can be a challenge when they are detected on the University of the West Indies Seismic Research Centre seismic network, so additional eyewitness observations are essential. Detailed studies of lahar deposits in the immediate aftermath are compromised by the rapid removal and cleanup response necessary to reduce disruption and allow population movement. The results presented in this study depend critically on numerous eyewitness reports of lahars captured on social media (including shared WhatsApp videos). These reports were mainly from people living in communities on the eastern side of the volcano and also increased in frequency after 23rd August 2021 when the all-clear was given for residents to return to the occupied areas on the volcano. Video sharing made use of connections made between residents and communities in the Changing Landscapes and VolcanoReady projects. These observations were vital in enabling us to compile a comprehensive record of lahar activity and also to test dynamic modelling to a high fidelity. In the future they will remain useful to augment instrumental data from the seismic network and rain gauges, and also provide additional information for understanding impacts at the community and infrastructure level, particularly at bridges and river fords in the north windward communities of St. Vincent. Continuing to build strong positive relationships with these communities will be critical for underpinning successful long-term lahar risk management in St Vincent.

Concluding Remarks

Lahars have been a persistent hazard on St Vincent since the April 2021 eruption of La Soufriere, with 25 recorded events in 2021 and ongoing activity, particularly in the rainy season. Typically, the lahars are relatively small volume, dilute or hyperconcentrated, weakly erosive and can occur on all flanks of the volcano. Daily rainfall of 20 mm local to a catchment can be sufficient to trigger a lahar event, although further work is needed to quantify the reliability of this as a threshold. Lahars are likely to be a significant hazard on St Vincent into the future, because of widespread ash deposition and vegetation damage on the flanks of the volcano caused by the the 2020-21 eruption of La Soufriere volcano.

The impacts of lahars have resulted in total losses estimated at US$12M. Most of the impacts have occurred to the primary coastal road and the communities in the northeast of St Vincent. Damage has been done to their drinking water supplies, road crossings and transportation and electrical distribution equipment. Hydro power plant has been affected by increased turbidity on both sides of the volcano. Damage to the road transport network has also hampered repairs to other infrastructure impacted.

Observations of lahars on St Vincent have been used to inform hazard modelling for both rapid identification of inundated areas using laharz, and computation of lahar properties and arrival times using the dynamic model LaharFlow. A simplified catchment hydrology approach using the 20 mm daily rainfall threshold seems to performs well in reconstructing a well-observed lahar event, and provides a basis for future more detailed hazard assessment.

Community observations of lahars communicated by social media have been vital in completing the record of lahar events, partly because instrumental detection of lahars by the seismic network cannot identify locations or flow properties. Engagement by scientists with affected communities has, in part, supported the creation of a Whatsapp group as a way of communicating occurrence and impacts of lahars across the northeast of St Vincent, which helps those communities reduce risk to life and manage disruption to transportation.

Acknowledgements

This research was partly funded by the 'Risk at the Margins' United Kingdom Research and Innovation Global Challenges Research Fund project EP/T024747/1. JCP acknowledges support from a University of Bristol Research Fellowship. Fieldwork for PDC and JB was funded by the Royal Society APX/R1/180094. We thank community members from the Changing Landscapes community group for their ongoing engagement and support with investigation of lahar occurrence and impacts in their communities. We thank Jennie Gilbert and Jim Vallance for their detailed and helpful reviews which have greatly improved our paper.

References

Barclay, J., Johnstone, J.E. and Matthews, A.J. 2006 Meterological monitoring of an active volcano: implications for eruption prediction. Journal of Volcanology and Geothermal Research.150:339-358 DOI:10.1016/j.jvolgeores.2005.07.020

Barclay, J., Alexander, J. and Susnik, J., 2007. Rainfall-induced lahars in the Belham valley, Montserrat, West Indies. *Journal of the Geological Society*, *164*(4), pp.815-827.

Baumann, V., Bonadonna, C., Cuomo, S., Moscariello, M. and Manzella, I., 2018. Slope stability models for rainfall-induced lahars during long-lasting eruptions. *Journal of Volcanology and Geothermal Research*, *359*, pp.78-94.

Castruccio, A. and Clavero, J., 2015. Lahar simulation at active volcanoes of the Southern Andes: implications for hazard assessment. *Natural hazards*, *77*(2), pp.693-716.

Chanson, H., 2004. *Hydraulics of open channel flow*. 2nd Edition, Elsevier, ISBN: 9780750659789

CHARIM, 2014. Caribbean Handbook on Risk Management. www.charim.net (accessed 03/05/2023)

Christie J., Barclay, J., Froude, M. and Bennett, G. (in prep) Multi-decadal landscape disturbance and lahar hazard in the Belham River Valley, Montserrat Geomorphology

Castruccio, A. and Clavero, J., 2015. Lahar simulation at active volcanoes of the Southern Andes: implications for hazard assessment. *Natural hazards*, *77*(2), pp.693-716.

Cole, P.D., Robertson, R.E.A., Fedele, L. and Scarpati, C., 2019. Explosive activity of the last 1000 years at La Soufrière, St Vincent, Lesser Antilles. *Journal of Volcanology and Geothermal Research*, *371*, pp.86-100.

Cole, P.D., Barclay, J. Robertson, R.E.A., Mitchell, S., Davies, B.V., Constantanescu, R., Sparks, R.S.J., Aspinall, W., Stinton, A. (this volume) Explosive sequence of La Soufriere St Vincent April 2021: insights into drivers and consequences via eruptive products.

Córdoba, G., Villarosa, G., Sheridan, M.F., Viramonte, J.G., Beigt, D. and Salmuni, G., 2015. Secondary lahar hazard assessment for Villa la Angostura, Argentina, using Two-Phase-Titan modelling code during 2011 Cordón Caulle eruption. *Natural Hazards and Earth System Sciences*, *15*(4), pp.757-766.

Darnell, A.R., Barclay, J., Herd, R.A., Phillips, J.C., Lovett, A.A. and Cole, P., 2012. Geographical information system approaches for hazard mapping of dilute lahars on Montserrat, West Indies. *Bulletin of volcanology*, *74*(6), pp.1337-1353.

Fiske, R.S. and Sigurdsson,H. (1982) Soufriere Volcano, St Vincent: Observations of its 1979 eruptoin from the Ground, Aircraft and Satellites. Science. 216: 1105-1006.

Forterre, Y., & Pouliquen, O., 2008. Flows of dense granular media. *Annu. Rev. Fluid Mech.*, *40*, 1-24.

Garcia-Martino, A.R., Warner, G.S., Scatena, F.N. and Civco, D.L., 1996. Rainfall, runoff and elevation relationships in the Luquillo Mountains of Puerto Rico. *Caribbean Journal of Science*, *32*, pp.413-424.

Gentile, R., Cremen, G., Galasso, C., Jenkins, L.T., Manandhar, V., Mentese, E.Y., Guragain, R. and McCloskey, J., 2022. Scoring, selecting, and developing physical impact models for multi-hazard risk assessment. *International Journal of Disaster Risk Reduction*, p.103365.

Government of St. Vincent and the Grenadines (2021a) La Soufriere Volcanic Eruption Sector Report.

Government of St. Vincent and the Grenadines (2021b) Post Disaster Needs Assessment – Water Sanitation and Hygiene (WASH) Sector Report, Central Water and Sewerage Authority.

Government of St. Vincent and the Grenadines (2021c) Detailed Damage Assessment Infrastructure and Housing – Effects of the La Soufriere Eruption Report, Ministry of Transport, Works, Lands & Physical Planning.

Griswold, J.P. and Iverson, R.M., 2008. *Mobility statistics and automated hazard mapping for debris flows and rock avalanches*. US Department of the Interior, US Geological Survey.

Hovey, E.O. (1909) Clearing out of the Wallibu and Rabaka gorges on Saint Vincent Island. Bull Geol. Soc. America: 20: 417-425

Iverson, R.M. and Ouyang, C., 2015. Entrainment of bed material by Earth-surface mass flows: Review and reformulation of depth-integrated theory. *Reviews of geophysics*, *53*(1), pp.27-58.

Iverson, R.M. and George, D.L., 2014. A depth-averaged debris-flow model that includes the effects of evolving dilatancy. I. Physical basis. *Proceedings of the Royal Society A: Mathematical, Physical and Engineering Sciences*, *470*(2170), p.20130819.

Iverson, R.M., Schilling, S.P. and Vallance, J.W., 1998. Objective delineation of lahar-inundation hazard zones. *Geological Society of America Bulletin*, *110*(8), pp.972-984.

iWitness News, 2022 (https://www.iwnsvg.com/2022/05/30/svg-preparing-for-hurricane-season-compounded-by-eruption-aftermath/), accessed on 03/05/2022.

Jenkins, S.F., Phillips, J.C., Price, R., Feloy, K., Baxter, P.J., Hadmoko, D.S. and de Bélizal, E., 2015. Developing building-damage scales for lahars: application to Merapi volcano, Indonesia. *Bulletin of Volcanology*, *77*(9), pp.1-17.

Jones, R., Manville, V. and Andrade, D., 2015. Probabilistic analysis of rain-triggered lahar initiation at Tungurahua volcano. *Bulletin of Volcanology*, *77*(8), pp.1-19.

Joseph, E.P., Camejo-Harry, M., Christopher, T., Contreras-Arratia, R., Edwards, S., Graham, O., Johnson, M., Juman, A., Latchman, J.L., Lynch, L. and Miller, V.L., 2022a. Responding to eruptive transitions during the 2020–2021 eruption of La Soufrière volcano, St. Vincent. *Nature communications*, *13*(1), pp.1-15.

Joseph, E.P., Robertson, R., Contreras-Arratia, R. and Stewart, R. 2022b. Scientific Advisories of the 2020-2021 eruption of La Soufriere volcano, St. Vincent. SRC Open File Report OFR 22-01, 16 March 2022, 394p.

Langham, J., Woodhouse, M.J., Hogg, A.J. and Phillips, J.C., 2021. Linear stability of shallow morphodynamic flows. *Journal of Fluid Mechanics*, *916, A31*.

Lavigne, F. and Thouret, J.C., 2003. Sediment transportation and deposition by rain-triggered lahars at Merapi Volcano, Central Java, Indonesia. *Geomorphology*, *49*(1-2), pp.45-69.

Leone, F., Komorowski, J-C., Gheradi-Leone,M. & Lalubie, G. (2019) Integrating spatial accessibility in the design of volcano evacuation plans in the French West Indies (Guadeloupe and Martinique). J Appl. Volc. 8: 8. https://doi.org/10.1186/s13617-019-0089-1

Longobardi, A., Villani, P., Grayson, R.B. and Western, A.W., 2003, July. On the relationship between runoff coefficient and catchment initial conditions. In *Proceedings of MODSIM* (pp. 867-872).

Mead, S., Magill, C. and Hilton, J., 2016. Rain-triggered lahar susceptibility using a shallow landslide and surface erosion model. *Geomorphology*, *273*, pp.168-177.

Mergili, M., Fischer, J.T., Krenn, J. and Pudasaini, S.P., 2017. r. avaflow v1, an advanced open-source computational framework for the propagation and interaction of two-phase mass flows. *Geoscientific Model Development*, *10*(2), pp.553-569.

Meyer-Peter, E. and Müller, R., 1948. Formulas for bed-load transport. In *IAHSR 2nd meeting, Stockholm, appendix 2*. IAHR.

Miller, V.L., Joseph, E.P., Sapkota, N. and Szarzynski, J., 2022. Challenges and Opportunities for Risk Management of Volcanic Hazards in Small-Island Developing States. *Mountain Research and Development*, *42*(2), pp.D22-D31.

Newhall, C.G. and Punongbayan, R. eds., 1996. *Fire and mud: eruptions and lahars of Mount Pinatubo, Philippines* (p. 1126). Quezon City: Philippine Institute of Volcanology and Seismology.

O'Brien, J.S., Julien, P.Y. and Fullerton, W.T., 1993. Two-dimensional water flood and mudflow simulation. *Journal of hydraulic engineering*, *119*(2), pp.244-261.

Ogden, F.L., 2016. Evidence of equilibrium peak runoff rates in steep tropical terrain on the island of Dominica during Tropical Storm Erika, August 27, 2015. *Journal of Hydrology*, *542*, pp.35-46.

Pierson, T.C., Janda, R.J., Thouret, J.C. and Borrero, C.A., 1990. Perturbation and melting of snow and ice by the 13 November 1985 eruption of Nevado del Ruiz, Colombia, and consequent mobilization, flow and deposition of lahars. *Journal of Volcanology and Geothermal Research*, *41*(1-4), pp.17-66.

Peruzzetto, M., Mangeney, A., Bouchut, F., Grandjean, G., Levy, C., Thiery, Y., & Lucas, A., 2021. Topography curvature effects in thin-layer models for gravity-driven flows without bed erosion. *Journal of Geophysical Research: Earth Surface*, 126, e2020JF005657. https://doi.org/10.1029/2020JF005657

Poulidis, A., Renfrew, I.A. and Matthews, A.J., 2016. Thermally induced convective circulation and precipation over an isolated volcano. J. Atmos. Sciences 73: 1667-1686

Richardson, J.F. and Zaki, W.N., 1954. The sedimentation of a suspension of uniform spheres under conditions of viscous flow. *Chemical Engineering Science*, *3*(2), pp.65-73.

Robertson, R., 2005. St. Vincent. *Volcanic Hazard Atlas of the Lesser Antilles*, pp.240-261.

Rodolfo, K.S., Umbal, J.V., Alonso, R.A., Remotigue, C.T., Paladio-Melosantos, M.L., Salvador, J.H., Evangelista, D. and Miller, Y., 1996. Two years of lahars on the western flank of Mount Pinatubo: Initiation, flow processes, deposits, and attendant geomorphic and hydraulic changes. *Fire and mud: eruptions and lahars of Mount Pinatubo, Philippines*, pp.989-1013.

Schilling, S.P., 2014. *Laharz_py: GIS tools for automated mapping of lahar inundation hazard zones*. US Department of the Interior, Geological Survey.

Sigurdsson, H. (1982) Tephra from the 1979 Soufriere Explosive Eruption. Science 216: 1106-1108.

Soulsby, R.L., 1997. Dynamics of marine sands: a manual for practical applications. *Oceanographic Literature Review*, *9*(44), p.947.

Sparks, R.S.J, Aspinall, W., Barclay, J., Refrew, I., Stewart, R. (This volume) Analysis of magma flux and eruption intensity during the explosive activity at Soufrière St Vincent.

Spearman, J. and Manning, A.J., 2017. On the hindered settling of sand-mud suspensions. *Ocean Dynamics*, *67*(3), pp.465-483.

Caribbean Conservation Association, 1991. St. Vincent and the Grenadines: country environmental profile. 222 p. NII Book ID: BA37293577

Tarolli, P., Borga, M., Morin, E., and Delrieu, G.: Analysis of flash flood regimes in the North-Western and South-Eastern Mediterranean regions, 2012. Nat. Hazards Earth Syst. Sci., 12, 1255–1265, https://doi.org/10.5194/nhess-12-1255-2012.

Taylor, M.A., Stephenson, T.S., Chen, A.A. and Stephenson, K.A., 2012. Climate change and the Caribbean: Review and response. *Caribbean studies*, pp.169-200.

Tierz, P., Woodhouse, M.J., Phillips, J.C., Sandri, L., Selva, J., Marzocchi, W. and Odbert, H.M., 2017. A framework for probabilistic multi-hazard assessment of rain-triggered lahars using Bayesian belief networks. *Frontiers in Earth Science*, *5*, p.73.

Vallance, J.W. (2000) Lahars. In: H. Sigurdsson, B.F. Houghton, S.R. McNutt, H. Rymer, and J. Stix (eds), *Encyclopedia of Volcanoes* (pp. 601–616). Academic Press, London.

Vallance, J.W., 2005. Volcanic debris flows. In *Debris-flow hazards and related phenomena* (pp. 247-274). Springer, Berlin, Heidelberg.

Vallance, J.W. and Iverson, R.M., 2015. Lahars and their deposits. In *The encyclopedia of volcanoes* (pp. 649-664). Academic Press.

Van Westen, C.J. and Daag, A.S., 2005. Analysing the relation between rainfall characteristics and lahar activity at Mount Pinatubo, Philippines. *Earth Surface Processes and Landforms*, *30*(13), pp.1663-1674.

Voellmy, A., 1955. Uber die zerstorungskraft von lawinen. *Bauzeitung*, *73*, 159-165.

Woodhouse, M.J., Johnson, C.G., Hogg, A.J., Phillips, J.C., Espin Bedon, P., Almeida, S. and Andrade, S.D., 2016. A model of lahars for hazard assessment. DOI:10.13140/RG.2.2.35597.95201

Yamakoshi, T., 2005. Post-eruption hydrology and sediment discharge at the Miyakejima volcano, Japan. Zeitschrift fur Geomorphologie, Supplement volume, 140, 55-72.

Figure Captions

Fig. 1 – Map of St Vincent, showing settlements, river channels, raingauges, hydropower plants and the volcano observatory referred to in the main text. 'SRC/CL' denotes the University of the West Indies/'Changing Landscapes' project, and 'CWSA' is the Central Water and Sewerage Authority of St Vincent and the Grenadines. North arrow shown in top left.

Fig. 2 – Timeline of lahar events from April to November. The length of the vertical bars corresponds to the amount of daily rainfall on the scale shown by the dotted lines, and the dates of days in which lahars were observed or instrumentally detected are shown as numbers within each month.

Fig. 3. – Syn and post eruptive Lahar Deposits. (a) Small lobes of syneruptive lahar deposits at the mouth of the Dry Wallibou valley , thought to be formed on 11th April 2021. (b) Lobes of syneruptive lahar deposits at the mouth of the Wallibou valley show concentrations of coarse scoria and wood debris, again considered to be formed on 11th April 2021. (c) Drone aerial view of surface of the syneruptive 11th April lahar deposit near the mouth of the Dry Wallibou valley, note dessication cracks (Photo taken on 26th April 2021). (d) Section through the 11th April 2021 lahar deposits at mouth of Wallibou valley. April 2021 tephra fallout layers form horizon below lahar level with persons chest. (e) Section in Wallibou valley showing massive 11th April Lahar deposits '1' with stratified 29th April and 3rd May lahars on top ('2'. upper Left hand side). (f) Detail of stratified deposits formed by 29th April /3rd May lahars.

Fig. 4 – Lahar flow in the Wallibou, 3rd May 2021. (a) Baseline flow, depth approximately 0.3 m, arrowed channel width is estimated in the range 15 – 30 m, flow velocity approximately 2 m s^{-1}. (b) A higher discharge pulse, with its flow front arrowed, depth approximately 1 m, flow velocity 3 m s^{-1}. Note the slightly different field of view of each image.

Fig. 5 – Locations of bridges and fords damaged by lahars following the April 2021 explosions. North arrow is shown in top left.

*Fig. 6 - Modelled distal lahar inundations (*Laharz*; Schilling 2014) for four input lahar volumes (*5.0 x 10^3, 5.0 x 10^4, 1.0 x 10^5, 5.0 x 10^5 m^3*). (a) Modelled lahar inundation for all catchments around the volcano; lahar hazard is confined to the north of St Vincent, the area of high volcanic hazard. North arrow is shown at top left (b) Inset from (a) showing modelled inundation of the Wallibou catchment highlighting that a volume of 5.0 × 10^4 m^3 is unable to reach the lower reaches of the channel, whereas a volume of 1.0 × 10^5 m^3 can easily propagate to the coastline; modified after Miller et al (2022).*

Fig. 7. The flow configuration for a model of a debris-laden flow down an inclined boundary varying in space and time. The dependent variables are the flow depth, $h(x,y,t)$, the flow velocity, $\mathbf{u}(x,y,t)$, the concentration of particles, $C(x,y,t)$ and the bed elevation, $b(x,y,t)$. The motion is driven by gravitational acceleration, g.

Fig. 8 – The Overland River catchment. The catchment area is shown within the solid white line as the semi-opaque polygon, and the location of the model source and road crossing observation point are shown as points 1 and 2, respectively. The direction of view is 300^o (North arrowed at top right).

Fig. 9 – 1st July 2021 lahar observed at the Overland River crossing. Flow is from left to right, and the channel width is approximately 20 m (courtesy RBS Broadcasting and Media Production, St Vincent and the Grenadines).

Fig. 10 - LaharFlow output overlaid on aerial imagery for a simulated lahar in the Overland River: (a) flow depth (m); (b) flow depth at the Overland crossing (m); (c) flow speed (m s^{-1}); (d) topographic change due to erosion and deposition (m). The simulation source condition is a three-point hydrograph with a peak source flowrate of 160 m^3 s^{-1} and a duration of 500 s, and output shown is 80 mins after initiation, when the flow reached the coast. Orientation of each image is the same, with a north arrow shown on (a) bottom right.

Table Caption

Table 1 – Lahar detection and rainfall in April to November 2021. Raingauge locations are shown on Fig. 1.

Date	Lahar location	Max rainfall on any raingauge (mm)	Location of that raingauge	Nearest raingauge to observed lahar	Rainfall measured (mm)
11/04/2021	Wallibou and Rabacca rivers	9.4	Montreal	Jennings	8.0
20/04/2021	Rabacca and other east coast rivers	20.8	Perseverence	Perservence	20.8
22/04/2021	Undetermined	5.8	Convent	N/A	
27/04/2021	Red and Orange zone rivers	57.8	Hermitage	Hermitage	57.8
28/04/2021	All valleys around Soufriere	115.5	Montreal	Jennings	92.7
29/04/2021	All valleys around Soufriere	82.2	Rivulet Agri	Jennings	15.6
03/05/2021	All valleys around Soufriere	84.6	Montreal	Jennings	70.5
04/05/2021	All valleys around Soufriere	5.8	Dallaway	Rabacca (Clinic)	0.5
05/05/2021	small lahars	11.3	Majorca	Jennings	4.1
05/06/2021	Sandy Bay, Rabacca, Wallibou	43.4	Jennings	Jennings	43.4
06/06/2021		26.4	Hermitage	Hermitage	26.4
07/06/2021		22.6	Majorca	Convent	10.2
02/07/2021	Richmond?	119.6	Dallaway	Hermitage	101.1
07/07/2021	Richmond	25.6	Montreal	Richmond Vale	3.4
16/08/2021	Lahars in most valleys around Soufriere	110.6	Rivulet Agri	Hermitage	65.8
20/08/2021	heavy rainfall - lahar signals	144.2	Convent	N/A	
21/08/2021	heavy rainfall - lahar signals	23.1	Hermitage	N/A	
22/08/2021	heavy rainfall - lahar signals	83.1	Richmond Vale	N/A	
23/08/2021	heavy rainfall - lahar signals	151.2	Hermitage	N/A	
24/08/2021	lahar signals	63.6	Bell Isle	N/A	
25/08/2021	lahar signals	Event in early hours, continuation of event on 24/08/21			
26/09/2021	lahar signals	53.9	Majorca	Belle Isle	30.2
11/10/2021	lahar signals	45.7	Botanic Gardens	Hermitage	44.8
18/10/2021	lahar signals	32.2	Rivulet Agri	Hermitage	8.4
31/10/2021	lahar signals	22.3	Dallaway	Hermitage	19.2
28/11/2021	lahar signals	44.9	Jennings	Hermitage	37.8

Table 1

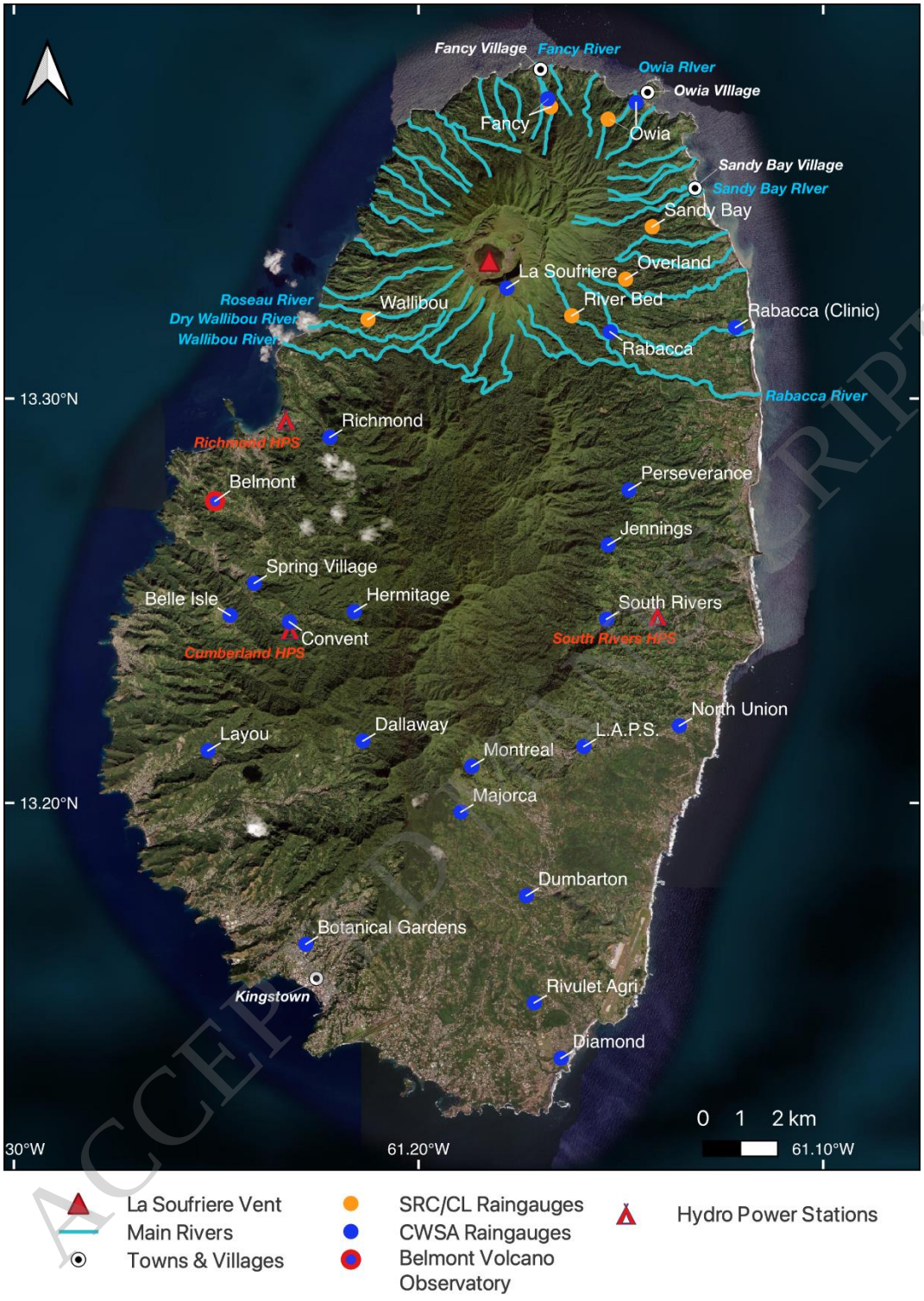

Figure 1

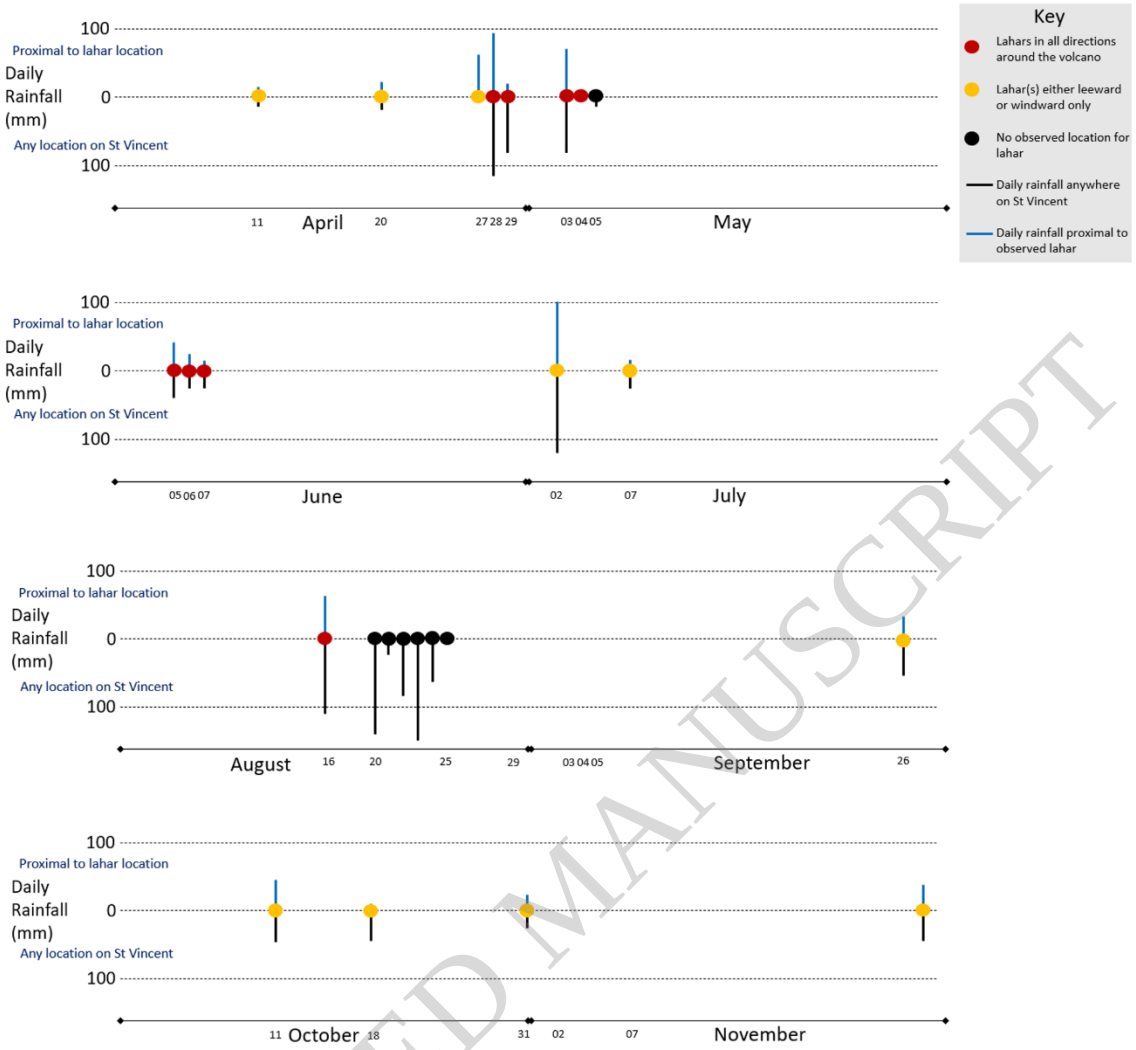

Figure 2

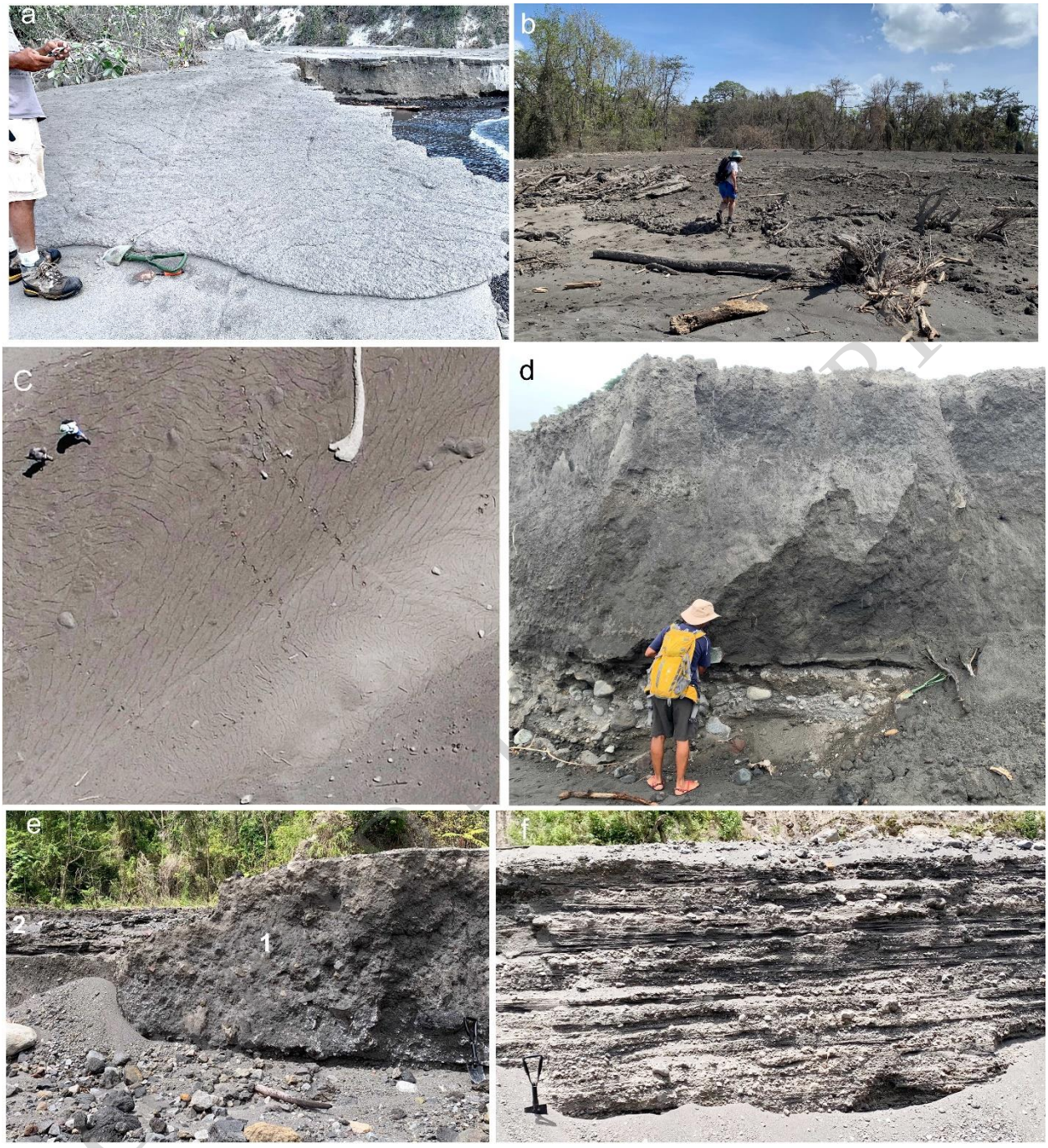

Figure 3

Figure 4

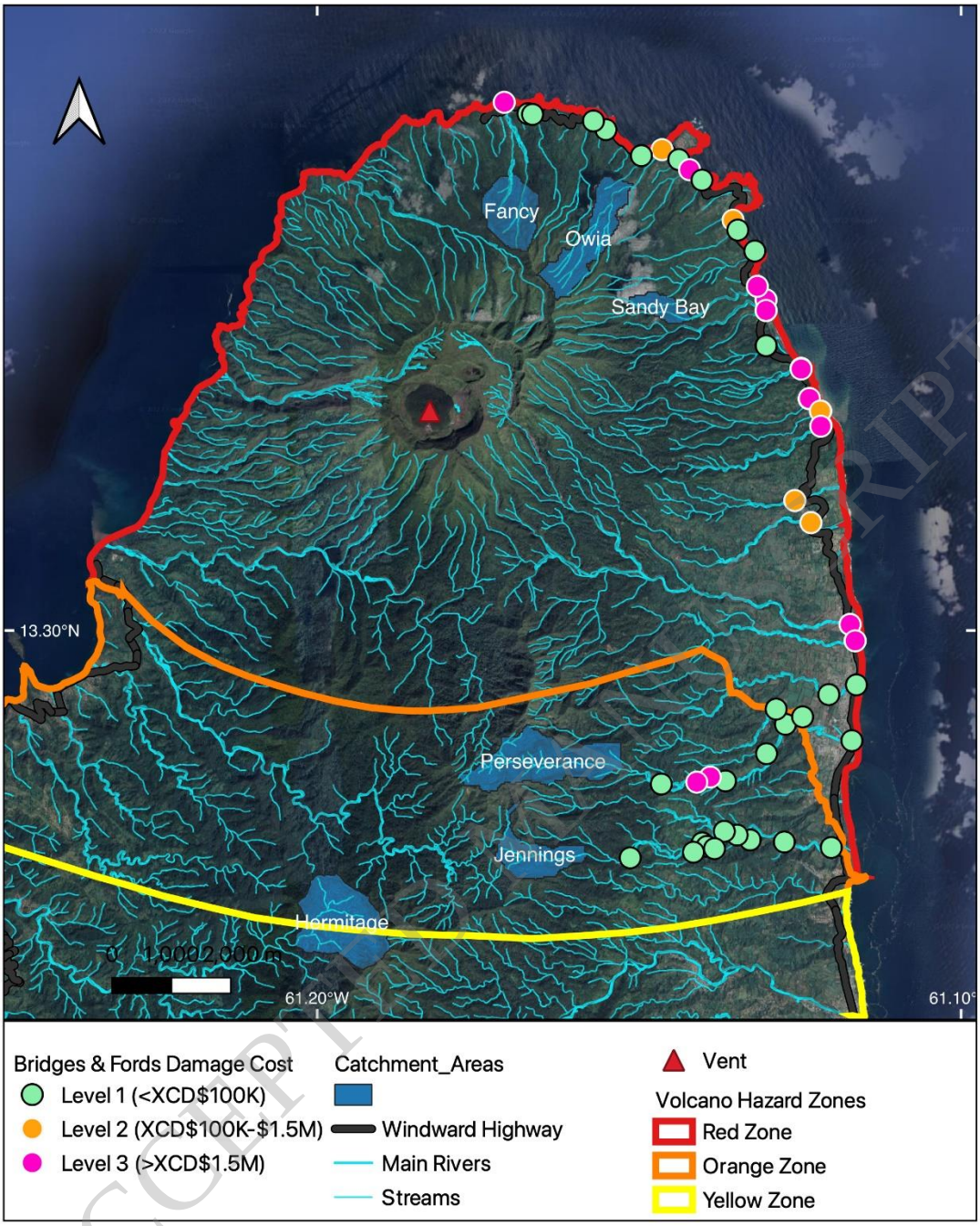

Figure 5

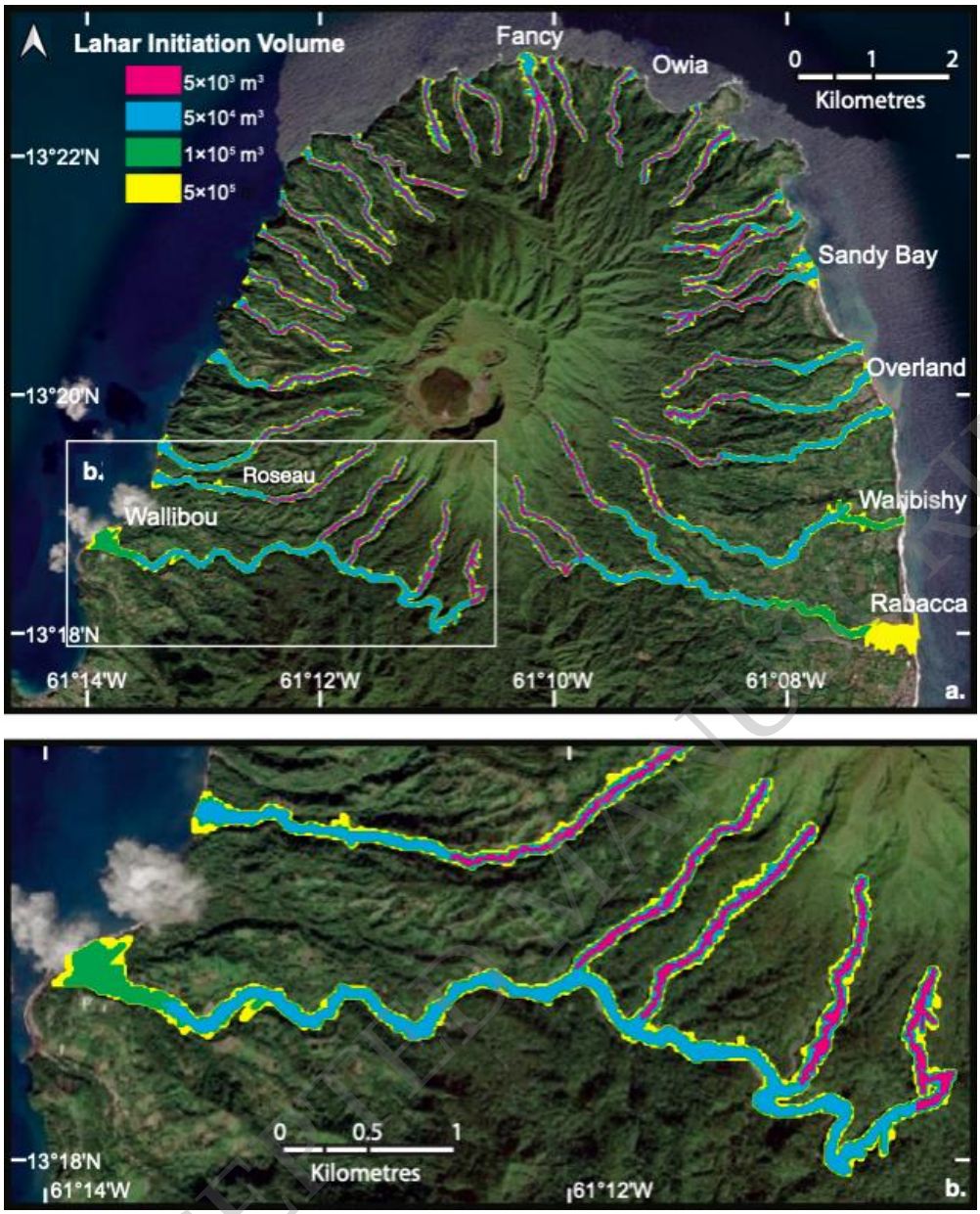

Figure 6

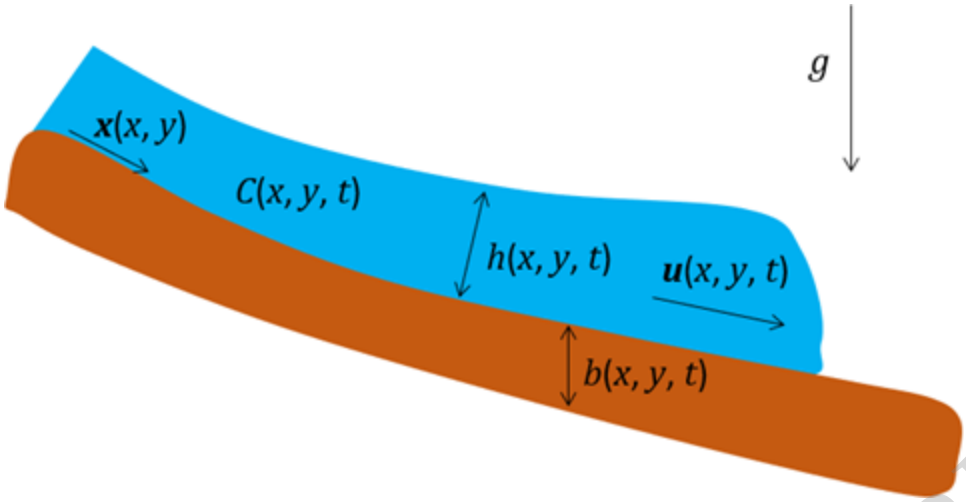

Figure 7

Figure 8

Figure 9

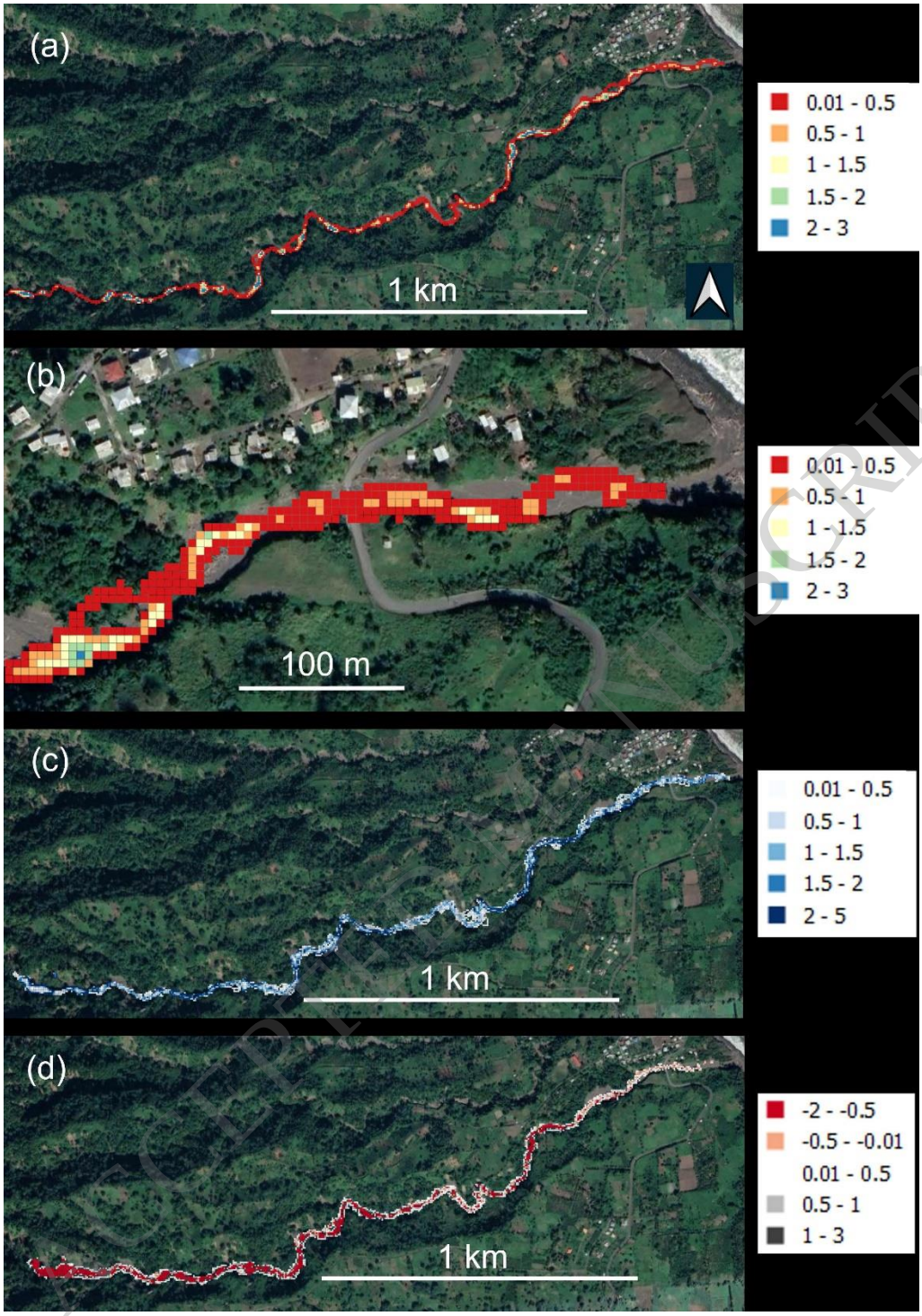

Figure 10